Environmental Science: Atmospheres

ROYAL SOCIETY OF CHEMISTRY

PAPER

View Article Online
View Journal | View Issue

Cite this: *Environ. Sci.: Atmos.*, 2022, **2**, 1152

Probing the impact of a phytoplankton bloom on the chemistry of nascent sea spray aerosol using high-resolution mass spectrometry†

Nikola Radoman, *[ab] Sigurd Christiansen, [ac] Jana H. Johansson, [a] Jeffrey A. Hawkes, [d] Merete Bilde,[e] Ian T. Cousins [a] and Matthew E. Salter [af]

Sea spray aerosol is the largest natural source of aerosol to Earth's atmosphere with significant impacts on climate. Despite this, estimates of the impact of sea spray aerosol on Earth's radiation budget are highly uncertain due to an overall lack of understanding of the physical and chemical factors controlling its composition. Critically, results from studies probing the importance of oceanic biological activity on the amount and type of organic matter present in nascent sea spray aerosol have been ambiguous. Some field studies have shown a relationship between the organic fraction of sea spray aerosol and oceanic primary productivity while others have reported no such relationships. Given this, we have probed the composition of seawater and nascent sea spray aerosol during a phytoplankton bloom in the North Atlantic using a novel liquid chromatography-mass spectrometry method. We observed that the composition of dissolved organic matter present in seawater changed as the phytoplankton bloom progressed over an 18 day period. Further, we observed changes to both the chemical composition of the organic matter present in seawater and the chemical composition of the organic matter present in the sea spray aerosol despite the organic matter mass fraction of the aerosol remaining unchanged. More specifically, we observed that the nascent sea spray aerosol became progressively more enriched in surface-active organic substances as the bloom progressed and that the sea spray aerosol had a distinct organic matter composition compared to the seawater. Thus, our work provides additional insight into the biological dependence of nascent sea spray aerosol composition.

Received 28th March 2022
Accepted 24th July 2022

DOI: 10.1039/d2ea00028h

rsc.li/esatmospheres

Environmental significance

How sea spray aerosol (SSA) impacts Earth's radiation budget is uncertain due to a lack of understanding of the physical and chemical factors controlling its composition. Critically, while some studies find a relationship between the organic fraction of SSA and oceanic primary productivity others do not. Here, we have used a novel liquid chromatography-mass spectrometry method to probe changes to the composition of the organic matter present in nascent SSA during a natural phytoplankton bloom. Interestingly, despite the organic matter mass fraction of the aerosol remaining unchanged during the sampling period we observed measurable changes in the composition of the organic matter present. This highlights the potential for biological activity in the oceans to impact the chemical composition of nascent SSA with potential implications for the role of SSA in regulating Earth's climate.

1 Introduction

Sea spray aerosol (SSA) particles dominate the mass fraction of natural particulate matter present in the global atmosphere[1] and exert a strong influence on radiation transfer,[2] cloud formation,[3] and atmospheric chemistry in remote marine regions.[4] SSA is formed during the process of bubble bursting following wave breaking[5] and decades of research have enabled a detailed description of the bubble-bursting process [*e.g.* ref. 5–10]. In short, hundreds of droplets are formed from a single bubble when the so-called bubble film-cap ruptures.[8] As such, these droplets are commonly referred to as film droplets[7] and the chemical composition of these droplets reflects the composition of the film-cap that the droplets were born from

[a]*Department of Environmental Science, Stockholm University, SE-106 91, Stockholm, Sweden. E-mail: nikola.radoman@aces.su.se*
[b]*Department of Materials and Environmental ChemistryStockholm University, SE-106 91, Stockholm, Sweden*
[c]*Faculty of Science and TechnologyUniversity of the Faroe Islands, FO-100, Tórshavn, Faroe Islands*
[d]*Department of Chemistry - BMCUppsala University, SE-751 24, Uppsala, Sweden*
[e]*Department of ChemistryAarhus University, DK-8000, Aarhus C, Denmark*
[f]*Bolin Centre for Climate Research, SE-106 91, Stockholm, Sweden*

† Electronic supplementary information (ESI) available. See https://doi.org/10.1039/d2ea00028h

ref. 11. Given this, the chemical composition of these droplets is often assumed to be similar to that of the air-sea interface or so-called "sea surface microlayer" [*e.g.* ref. 12 and 13]. The retraction of the bubble film-cap following rupture exposes a cavity and results in the formation of a jet which originates at the base of the cavity.[14] Destabilization of this jet results in the formation of droplets which are commonly referred to as jet droplets.[15] The consensus view is that these jet droplets are fewer in number concentration and much larger (*i.e.* >1 μm) than film droplets.[7,16] However, this view has recently been challenged by measurements which indicate that jet droplet production can produce large number concentrations of submicron particles.[17] With regards to their chemical composition, the conventional view is that jet droplets reflect the composition of the bulk surface ocean, rather than the interfacial region [*e.g.* ref. 11 and 17].

That nascent SSA is a complex mixture of sea salt and organic matter has also been known for decades [*e.g.* ref. 7]. Under certain conditions, organic matter has been shown to comprise a substantial fraction of the total particle mass, especially for those particles with diameters less than 1 μm, and, on a global scale, upwards of 8 Tg y^{-1} of primary submicrometer organic aerosol is estimated to originate as SSA[18,19] which can be compared to global emission estimates of 34–144 Tg y^{-1} of total primary organic aerosol.[20] Indeed, it is well established that the organic mass fraction of SSA and aerosol diameter are inversely proportional [*e.g.* ref. 21–24] with observations of organic carbon mass fractions of upwards of 0.9 for dried SSA particles of around 100 nm in diameter.[24] Given that oceanic surface waters usually have organic mass fractions of far less than 0.0001 (ref. 25) it is clear that organic matter is significantly enriched in these smaller particles and it is likely that the formation process of film droplets is responsible for this enrichment.[12,13]

Understanding the temporal and spatial variability in the amount and type of organic matter present in nascent SSA is critical if efforts to reduce the current uncertainty in estimates of the impact of SSA on the Earth's radiation budget are to be successful. For example, the amount of organic matter in SSA may impact its radiative properties [*e.g.* ref. 26]. The organic mass fraction as well as the chemical composition, morphology and phase state [*e.g.* ref. 27] of SSA affects its ability to act as cloud condensation nuclei [*e.g.* ref. 28] and ice nuclei [*e.g.* ref. 29].

Ever since the initial studies concerned with the enrichment of organic matter in nascent SSA, the role of biological activity in oceanic surface waters on the quantity and composition of organic matter in SSA has been an important question [*e.g.* ref. 30]. Numerous studies investigating the impact of the biogeochemical state of the ocean on nascent SSA have been conducted (see for example the recent review by Bertram *et al.*[31] and their Table 1) and the conclusions of these works can generally be characterised as falling into two camps. Firstly, a series of studies have observed that the organic carbon (OC)/Na^+ ratios of either ambient marine aerosol [*e.g.* ref. 24] or nascent SSA [*e.g.* ref. 32 and 33] are highly dependent on the level of biological activity (*e.g.* the amount of phytoplankton present in the ocean) with lower OC/Na^+ ratios during periods of low biological activity compared to periods of high biological activity. In support of the argument that much of the organic matter present in nascent SSA results from recent biological activity, O'Dowd *et al.*[24] observed that the water-insoluble organic matter (WIOM) fraction of ambient aerosol obtained at Mace Head in the Eastern North Atlantic increased significantly during periods influenced by phytoplankton blooms relative to the water-soluble organic matter (WSOM) fraction. Similarly, Van Pinxteren *et al.*[34] observed the highest concentration of WIOM in submicron ambient marine aerosols over the North Atlantic during high chlorophyll-a conditions. In contrast, the second group of studies have observed little difference in the OC/Na^+ ratio of nascent SSA when comparing oligotrophic and productive oceanic regions [*e.g.* ref. 35 and 36] or during mesocosm phytoplankton experiments.[37] Instead, these studies generally argue that the ubiquitous reservoir of organic carbon in surface seawater is responsible for the organic carbon enrichment of nascent SSA, overwhelming any influence of local biological activity.

Numerous studies have investigated the impact of ocean biology on the SSA organic composition of SSA. Gerard *et al.*[38] observed a correlation between the concentration of both anionic and cationic surfactants in ambient coastal Baltic SSA with chlorophyll-a – levels, which was indicative of their marine and biogenic origin. These surfactants were shown to modulate the surface tension of the SSA, and it was assumed this may impact their CCN properties. Frossard *et al.*[39] found that a higher concentration of naturally occurring surfactants in the SSA that was generated from productive seawater compared to oligotrophic water, indicating biological impact on SSA chemical properties. Studying the temporal trends in SSA generated from microcosm plankton blooms, Santander *et al.*,[40] concluded that sea-to-air transfer of different chemical species did not correlate with plankton growth and chlorophyll-a levels but it is more likely related to more complex processes such as bacterial transformation and degradation of plankton primary products.

Carbon isotope measurements have also been used to investigate links between oceanic primary productivity and the composition of SSA. For example, Ceburnis *et al.*[41] found that most organic enrichment in marine aerosol over the southern Indian Ocean was attributable to fresh particulate organic matter. In line with these findings Crocker *et al.*[42] observed that the carbon isotopic composition of nascent laboratory-generated SSA reflected changes in seawater composition during mesocosm phytoplankton blooms while Beaupré *et al.*[43] recently reported that highly aged dissolved organic matter (DOM) carbon could account for 19–40% of the organic carbon in artificially generated sea spray using seawater from the northwest Atlantic suggesting that younger, recently produced carbon could account for the majority.

A series of studies have characterised the organic matter in SSA, often with a focus on specific organic fractions or specific classes of compounds [*e.g.* Table 2 in ref. 44]. NMR (nuclear magnetic resonance) analysis of ambient aerosol obtained at Mace Head revealed that the majority of the WSOM was comprised of humic-like compounds that contain keto and

carboxyl functional groups combined with aliphatic moieties.[45] Containing both polar groups and aliphatic chains, these structures are assumed to possess surface-active properties that enable them to be enriched in SSA. By using Raman microspectroscopy (RMS), Deng *et al.*[46] observed the prevalence of long-chain aliphatic organic compounds with different functional groups in SSA collected across the Pacific Ocean during both spring and autumn seasons. Facchini *et al.*[32] probed the chemical properties of nascent SSA produced *via* artificial bubble bursting experiments with oceanic waters obtained during a phytoplankton bloom in the North Atlantic. During these experiments the authors observed a prevalence of WIOM with characteristic lipopolysaccharide compounds, which likely originated from phytoplankton exudates. During the same experiments the WIOM and WSOM showed similar composition based on NMR profiles, with WIOM having more long hydrophobic chain lipids and sugars compared to the WSOM. Russell *et al.*[35] analysed the chemical composition of aerosols obtained over the North Atlantic and observed a strong carbohydrate FTIR (Fourier transform infrared spectroscopy) signature characteristic of saccharides which are known to be highly abundant in surface seawater. Utilising the same FTIR analysis of functional groups, Frossard *et al.*[44] observed a higher abundance of alkane functional groups in nascent laboratory-generated SSA using biologically productive water compared to less biologically productive water.

High-resolution mass spectrometry facilitates the analysis of all the ionisable compounds within DOM simultaneously, with typical mass spectra consisting of thousands of molecular ions, each being assigned with a different molecular formula.[47–49] However, the number of structural isomers behind every molecular formula is still undefined[50–52] to the extent that analysis of these compounds remains extremely challenging. A typical analytical workflow includes solid-phase extraction of marine DOM [*e.g.* ref. 53], followed by direct infusion of the extracts into a Fourier-transform ion cyclotron resonance mass spectrometer (FT-ICR-MS) [*e.g.* ref. 48 and 54]. More recently, characterisation of DOM has been performed using Orbitrap mass spectrometry.[55,56] Analysis of DOM by coupling of mass spectrometry with liquid chromatography has been performed with Orbitrap[57,58] and more recently also with FT-ICR-MS [*e.g.* ref. 59 and 60].

Although high-resolution electrospray ionisation mass spectrometry has previously been used to characterise water-soluble organic compounds in nascent laboratory-generated SSA[61,62] and ambient marine aerosols,[63] the number of studies is limited. The studies by both Schmitt-Kopplin *et al.*[61] and Willoughby *et al.*[63] revealed that CHO molecular formulas with low O/C and high H/C molecular ratios were most abundant which is indicative of biological input of lipid-like compounds suggesting that changes in the composition of seawater due to biological activity may be reflected in nascent SSA.

In the current study we have used high-resolution mass spectroscopy to examine compositional changes in the DOM present in subsurface water, sea surface microlayer and nascent SSA during the spring phytoplankton bloom in the North Atlantic with a view to furthering our understanding of the role marine primary productivity plays in shaping the chemical composition of nascent SSA. Further details of the campaign can be found in Christiansen *et al.*[64]

2 Experimental

The samples used in this study were collected during a 3 week field campaign on the Faroe Islands in June 2019 (June 4th–June 23rd 2019). The campaign is described in detail by Christiansen *et al.*[64] and the conditions are summarised only briefly here.

Situated between Scotland and Iceland, the Faroe Islands (62°N, 7°W) are an archipelago with a shelf ecosystem, surrounded by open ocean (Fig. S1†). Given that the areas surrounding the Faroe Islands are dominated by North Atlantic seawater, the sampling location is considered representative of the region as a whole with a homogeneous water mass without summer stratification.[65] The seawater inlet used during the campaign has been used in numerous studies to obtain samples for the analysis of temporal trends in zoo- and phytoplankton on the Faroes shelf.[66–69] The seawater inlet used during the campaign is situated within a sound characterised by strong tidal currents which represents the oceanic conditions on the Faroe Island central shelf well.[67] As such, minimal variation in both temperature and chlorophyll-a values occur down to 50 m depth.[66]

The timing of the sampling campaign was chosen to match the North Atlantic spring bloom when net primary productivity exceeds the loss of phytoplankton biomass to grazing and mortality, leading to transient net biomass accumulation and a peak in phytoplankton abundance.

2.1 Generation of nascent sea spray aerosol

SSA was generated using the Aegor sea spray simulation chamber developed by Christiansen *et al.*[70] which was continuously fed with fresh seawater between June 4th and June 23rd 2019 as presented in ref. 64. Seawater was fed from 18 m depth into a well which forms part of a fish broodstock facility.[66] From the water well, which stands on the seawater level below the facility, the seawater was pumped into the large indoor water pool from which seawater was passively directed to the lower level of the facility where SSA experiments were conducted. The sea spray chamber was supplied with that seawater through a reservoir tank with a centrifugal pump which supplied a continuous flow of 4 L min^{-1} through a jet flow nozzle into the sea spray chamber (Fig. S2†). The Aegor sea spray chamber is a stainless steel, cylindrical 36 L (29 cm inner diameter) tank, with a jet flow nozzle (4 mm in diameter) placed in the center of the top lid.[70] The sea spray chamber contained a seawater overflow outlet which was positioned to keep a constant water volume of 20 L (29 cm depth) and a headspace volume of 13.9 L (21 cm depth). All fittings were stainless steel and, where required, only silicon O-rings were used to minimise potential for chemical contamination. Particle-free sweep-air was continuously added into the headspace at a flow rate of 26–27 L min^{-1} which was slightly higher than the rate at which the aerosol sampling instruments withdrew air from the chamber.

This excess was vented through an overflow outlet in the headspace of the chamber and prevented potential contamination by ambient air in the factory facility where experiments were conducted.

2.2 Aerosol sampling

Aerosol-laden air from the sea spray chamber was directed to a 14-stage cascade impactor (DLPI+, Dekati) at 10 L min^{-1} through 50 cm of 10 mm stainless steel tubing. The aerosol was not dried and the average and standard deviation of the relative humidity measured in the headspace of the sea spray chamber was 71.4 ± 3.1% during impactor sampling. Humidity can influence the size distribution of the SSA that is being sampled on different stages of the impactor, but since we pooled all 14 stages in just 2 size fractions this probably didn't have much effect on our results. The cutoff sizes ($d50$) of the stages, which were calibrated by the provider (Dekati) of the impactor based on Järvinen *et al.*[71] ranged from 0.015 to 9.91 μm ($d50$s: stage 2 – 0.0150, stage 3 – 0.0306, stage 4 – 0.0548, stage 5 – 0.0944, stage 6 – 0.154, stage 7 – 0.256, stage 8 – 0.383, stage 9 – 0.605, stage 10 – 0.951, stage 11 – 1.64, stage 12 – 2.48, stage 13 – 3.67, stage 14 – 5.38, stage 15 – 9.91 μm). Each stage was loaded with a polycarbonate membrane (Nuclepore TrackEtch Membrane, Whatman), that were not pre-cleaned prior to the sampling. Due to the low mass of aerosol expected on the lower stages of the impactor the stages were pooled into two samples following each sampling period – a submicron sample which contained stages 2–10 ($d50$s: 0.0150–0.951 μm) and a supermicron sample which contained stages 11–15 ($d50$s: 1.64–9.91 μm). Preparation of the impactor for the chamber experiments and transfer of the polycarbonate membranes into precombusted total organic carbon (TOC) vials after the experiments were conducted in a glove box to avoid ambient air contamination. Handling blanks for SSA samples were obtained in the field by placing polycarbonate membranes on random impactor stages. In total, three handling blanks were collected and analysed (from the start, end and middle of the campaign), each containing four polycarbonate membranes from four different impactor stages. Once unloaded from the impactor, these membranes were treated in exactly the same fashion as the membranes exposed to the aerosol sample. Table S1† summarises the experiments conducted.

2.3 Seawater sampling

Subsurface water (SS) was sampled into 40 mL precombusted glass vials (450 °C for 4 h), through a tap located on the bottom of the chamber. In order to obtain samples from the air–water interface of the seawater used to generate sea spray aerosol we have used the glass plate method that is traditionally used to obtain sea surface microlayer samples.[72] Given this, we refer to these samples as sea surface microlayer (SML) samples throughout this study. However, it should be noted that the design of the sea spray chamber precluded the collection of sea surface microlayer (SML) samples from within the sea spray chamber using the glass plate method. Therefore, to enable sample collection these samples were collected from an open-top polyethylene container (380 L) that was filled continuously with seawater from the same well which supplied the sea spray chamber. The water flow of ~58 L min^{-1} was directed vertically to the water surface in the form of a plunging jet from the opening of the hose that was fixed at a height of approximately 20 cm above the water level. The plunging jet flow resulted in the entrainment of a significant amount of air followed by rising bubbles and a certain amount of foam on the water surface. The residence time of the seawater in the container was estimated to be 5–6 min so that excess seawater drained evenly over the top rim of the container. The SML sampling was done in proximity to the plunging jet and rising bubbles. A PTFE scraper was used to remove SML adhering to the glass plate and both the glass plate and the scraper were precleaned using HPLC-grade methanol. Foam was collected from the surface of the large indoor water pool from which water was withdrawn to supply the sea spray chamber. This foam likely formed as a result of strong turbulence occurring as the water was pumped from the well into the pool. In addition to this, a certain amount of foam was also observed in the headspace of the SSA chamber and during SML sampling. The moist upper layer of the foam was removed prior to sampling and fresh foam was sampled using a pre-cleaned 500 mL glass beaker. Following collection the beaker was covered with aluminum foil while the foam was left to settle. After approximately 10 min the foam sample was gently agitated by hand so that the foam and the small layer of surface water that was sampled together with the foam became homogeneous. Next the contents of the beaker were transferred into 40 mL precombusted glass vials. All three types of samples were acidified with concentrated HCl to 0.01 M immediately after sampling in order to increase the extraction efficiency and improve the recovery rate of the DOM present during subsequent solid phase extraction (SPE).[53]

2.4 Sample preparation

Each set of pooled polycarbonate impactor membranes were ultrasonicated for 20 min in 40 mL ultrapure water and the extracts were further acidified using 0.01 M HCl to approximately pH 2. From this point onwards the SS, SML and foam samples along with the aerosol extracts were all treated identically. Organic matter was extracted using an established solid phase extraction (SPE) procedure.[53] The procedure uses Bond Elut PPL cartridges (Agilent), containing styrene–divinylbenzene polymer sorbent which retains on average 62% of DOM from seawater [Dittmar *et al.*, 2008]. While it is known that PPL overall retains a similar range of compounds as C18 sorbent, it exhibits overall higher recovery and improved retention of N-containing compounds that potentially represent plankton-origin amines [Dittmar *et al.*, 2008]. 30 mL of the acidified subsurface water, SML samples, foam samples or the aerosol extracts were passed through the cartridges. The cartridges were then rinsed with 20 mL of acidified ultrapure water (0.01 M HCl) to remove salts which may interfere with the analysis, and dried with nitrogen gas. Organic matter was eluted from the dry sorbent with 2 mL of HPLC Chromasolv grade methanol (Honeywell Riedel-de Haen). Extracts were then reduced to

dryness by gently blowing off the solvent with dry nitrogen gas and then reconstituted in 300 μL of a 1 : 1 (v/v) mixture of methanol and ultrapure water. Parallel with extraction of the samples, procedural blanks were also obtained by following the same SPE procedure without applying the sample. None of the samples were filtered prior to sample preparation in order to avoid the risk of potential adsorption of surface-active compounds to the filter material. SS and SML samples didn't contain any visible particulate or colloidal particles. Any particulate material is likely to stay on the top of sorbent material but we cannot rule out the possibility that some organic compounds from the particulate phase were dissolved during the elution with methanol.

2.5 Organic matter characterisation using ultra-high-resolution mass spectrometry

Chromatographic separation was carried out on a Dionex UltiMate 3000 Ultrahigh performance LC (Thermo Scientific). 20 μL of the samples were injected onto a C18 Hypersil GOLD Polar Endcapped column (100 × 2.1) mm with a 1.9 μm bed size and 175 Å pore size (Thermo Scientific). Stepwise elution was performed using a mobile phase (0.3 mL min^{-1} flow) which changed from ultrapure water with 0.1% formic acid (mobile phase A) to 100% acetonitrile (mobile phase B), with the gradient profile described in Table S3.† The ultra performance liquid chromatography system was coupled to a Q Exactive HF hybrid Quadrupole-Orbitrap MS (Thermo Scientific). Negative ions were produced using an electrospray ionisation source using a −3 kV spray voltage, 320 °C capillary temperature, a sheath gas flow rate of 30 mL min^{-1} and a S-lens radio frequency level of 55%. Approximately 1700 high-resolution scans were collected over a period of 18 min for each LC-MS run, using an instrumental resolution of 240 000 (at m/z = 200) and a mass range from 150–1000 m/z.

2.5.1 Formula assignment and data analysis. Collected spectra were grouped into three retention time bins corresponding to three main polarity fractions: fraction A = 3–6 min, fraction B = 6.3–9 min and fraction C = 10–13 min. In reversed-phase liquid chromatography, the order of elution mostly depends on the affinity of the compound to the non-polar stationary phase. As such, fraction A, which elutes first, represents the most polar fraction while fraction C, which elutes last, represents the least polar fraction. The assignment of molecular formulas to m/z peaks was carried out using the R software package MFAssignR[49] which consists of several main functions. Removal of background noise peaks was carried out using the "KMDNoise" function, which is a modified method of Riedel and Dittmar.[73] Only analyte peaks with a signal-to-noise ratio greater than five were considered. The next step included preliminary assignments of the most abundant molecular formula containing C, H and O from which the ten most "reliable" homolog series were chosen as recalibration candidates. Recalibration candidates are optimised for each type of sample individually. The "Recal" function was set with the two most abundant recalibration candidates within each 10 m/z window, after which they were grouped in to 50 m/z windows across the entire m/z range. For each 50 m/z window the function calculated individual recalibration values based on a polynomial central moving average, using a method modified from Savory *et al.*[74] and Kozhinov *et al.*[75] After recalibration of the entire m/z set final formula assignment was conducted, allowing only CHO, CHON and CHOS formulas, with the maximum allowable error = 1 ppm, maximum allowable O/C = 1, and minimum allowable H/C = 0.3. CHO, CHON and CHOS formulas represent the most abundant fraction of formulas that can be identified in common marine DOM samples.[48] These peaks can be resolved with the maximum resolution offered by Orbitrap instruments while resolving molecular formulas that contain more heteroatoms (for example phosphorus or multiple S atoms) would require stronger resolving power.[55,56] For the compounds above 600 Da, formula assignment was only allowed if the formula belonged to the homolog series identified below 600 Da. Contamination ions were identified using the procedural and handling blanks as all ions higher than 0.1% of the intensity of the highest intensity blank peak. All contamination ions were removed from the final dataset. For each ion in the mass spectra that is assigned with a molecular formula we use the term "compound" although each peak likely represents the sum of different structural isomers which cannot be separated during chromatographic fractionation.[50,51,57,58]

After formula assignment, ion intensities were normalised by the sum of intensities of all identified ions in order to correct for instrumental drift or variations in SPE recovery. The repeatability of the measurements was estimated by injecting one SS sample five times throughout the LC-MS run and subsequent calculation of the Bray–Curtis Dissimilarity (BCD) between replicates as well as the relative standard deviation (RSD) of the relative abundances of the ions identified. Due to significantly different sampling times for the SSA experiments (from 20 to 36 h), we evaluated the repeatability of these samples by injecting different volumes (5–20 μL) of the samples (Table S4†). Of the different polarity fractions, those that were the most abundant for each sample type had the highest repeatability. For example, the SS samples exhibited the highest repeatability for fractions A and B (mean BCD coefficients 1–2%) while the SSA samples exhibited better repeatability for fraction C with a mean BCD coefficient between replicates of 3.1% (Table S5†).

Replicate measurements of supermicron SSA samples were also used to strengthen the molecular formula assignment; assignments were only accepted if they were achieved in at least two (or three) of the different volumes injected when three (four) discrete volumes were injected.

In order to explore whether the bloom had any impact on the composition of the DOM present in our samples we have used Spearman correlation rank to investigate the relationship between sum-normalised ion intensities and seawater chl-a level for each polarity fraction of each sample type. The ion intensity for each molecular formula in a given fraction was normalised relative to the sum of ion intensities of all identified ions in that fraction. For both SS and SML samples, relative ion intensities and chl-a concentrations from 11 different samples were correlated (Table S2†). For supermicron SSA samples,

relative ion intensities measured from 18 replicate injections from 6 different chamber experiments were used, while for submicron SSA samples that were analysed with no replicate injections, 6 data points were used (Table S4†). Since the chamber experiments usually covered 2 or 3 consecutive days (Table S1†), the chlorophyll concentration used in the correlation of SSA data was the average value for the given period.

2.5.2 Mass spectrometric fragmentation experiments. In order to probe the functional groups present we conducted mass spectrometric fragmentation experiments. To do so a m/z range from 395.00–412.40 was isolated *via* quadrupole and then fragmented *via* higher energy collision dissociation (HCD) with 35 V collision energy in the C-trap of the Orbitrap. The MS2 spectra from 50–440 m/z were then recorded with an instrumental resolution of 240 000. The mass range around 400 Da was chosen because it contains ions with high abundances for all polarity fractions (Fig. S8†), and the exact range of 17.4 Da was chosen so that neutral loss of water (18.01056 Da) for the compounds at the higher end of the m/z range would not overlap with some of the precursor ions at the lower end of the m/z range. For a given mass range (395.0–412.4 Da) there are 441 theoretical molecular masses of CHO compounds with the following criteria: H/C = 0.3–2, O/C < 1, double-bond equivalents (DBE; number of rings plus double bonds to carbon) minus oxygen (DBE-O) = −10 to 10. N and S containing formula were not considered in the data analysis due to their lower abundances compared to CHO compounds. For each precursor, 17 potential neutral losses were considered: losses of H_2O, losses of 1–6CO_2, losses of 1–6CO_2 + 1H_2O and losses of 1–3CO_2 + 1CH_3OH. In total, the theoretical mass list of 10 404 masses (441 precursors + 17 × 441 fragments) were matched with a mass list from the recorded MS2 spectra, which was collected separately for the same 3 retention time bins that correspond to the polarity fractions *A*, *B* and *C*, with a maximum error deviation of 3 ppm from the theoretical mass. Only fragments that were detected in more than 50% of the SS samples (minimum in 6 out of 11 samples), and in at least 75% of injected SSA samples (minimum in 3 out of 4 samples from sea spray chamber experiments 3–6), and whose intensity was at least five times higher than the estimated noise level and ten times higher than the blank intensity were evaluated further.

3 Results and discussion

3.1 Differences in DOM composition between subsurface seawater, sea surface microlayer, foam and nascent sea spray aerosol samples

Fig. 1 presents a comparison of compounds classified as DOM identified for each polarity fraction in the SS, SML, foam and SSA samples collected on the 21st of June 2019. Here, the top panel presents the total ion chromatograms which represent the sum of all detected ions' intensities, including both assigned and unassigned sample compounds, while the van Krevelen diagrams in the lower part of the figure include only those compounds whose molecular formula has been assigned according to the criteria described in Section 2.5.1.

Comparing across the three polarity fractions, there are clear differences between the sample types. In the SS and SML samples the highest number of assigned ions were observed in the more polar fractions *A* and *B* where the relative intensities are some 100 times higher than in the least polar fraction *C*. In contrast, the least polar fraction, *C*, was much more abundant than the more polar fractions *A* and *B* in the foam as well as the submicron and supermicron SSA samples, both in terms of the number of assigned ions and their relative intensities.

Although this comparison is just for a single day of the campaign the differences between the samples are representative of the campaign as a whole. This is shown in the Fig. S5,† where average van Krevelen diagrams for all samples are shown (only compounds that were present in 10 out of 11 SS and SML samples and in 5 out 6 SSA samples are included). Here a similar pattern to that observed on June 21st is also observed. Notably while those compounds presented in Fig. S5† (those compounds present in 10 out of 11 SS and SML samples and in 5 out 6 SSA samples) only represent approximately 2/3 of the total number of ions assigned with molecular formula, they account for a high percentage (82–99%) of the total ion intensity (Table S6†).

The SS and SML samples appear very similar in relative abundances of different polarity fractions and are clearly distinct in comparison to the foam and SSA samples. However, there are slightly more least polar compounds (fraction *C*) and slightly fewer polar and intermediate-polarity compounds (fraction *A* and *B*) in the SML samples compared to the SS samples. An explanation for the similarity of the SS and SML samples is dilution of the SML with underlying subsurface water. However, it may also be due to the fact that the water from which the SML was sampled originated at 18 m depth.

The composition of the foam sample is intermediate between the SML and SSA. The intermediate polarity fraction *B* is more abundant in the foam sample than in the SSA sample while the least polar fraction *C* is more abundant in the foam sample compared to the SML sample. Since the foam was scooped from the surface of the seawater it is unsurprising that it contains both intermediate polarity substances originating from subsurface seawater as well as an abundance of surface-active compounds that we think are concentrated in fraction *C* (explained further in this section). Indeed, the presence of more surface-active substances in the foam sample compared to the SML sample supports the idea that the foam is a concentrated SML.[76] Formation of foam is common during phytoplankton blooms, due to the large amount of surface-active substances originating from phytoplankton exudates, marine bacteria and organic detritus. This surface-active material is likely to be a complex mixture of biogenic lipids, polysaccharides and proteinaceous material.[77,78]

The submicron and the supermicron SSA samples, compared to all other samples, contain the highest number of compounds in the least polar fraction *C*, which we think is the polarity fraction with the most expressed surface-active properties. Comparison of the two SSA fractions reveal that the submicron size fraction of the SSA exhibited much lower ion abundances and fewer assigned formulas compared to the

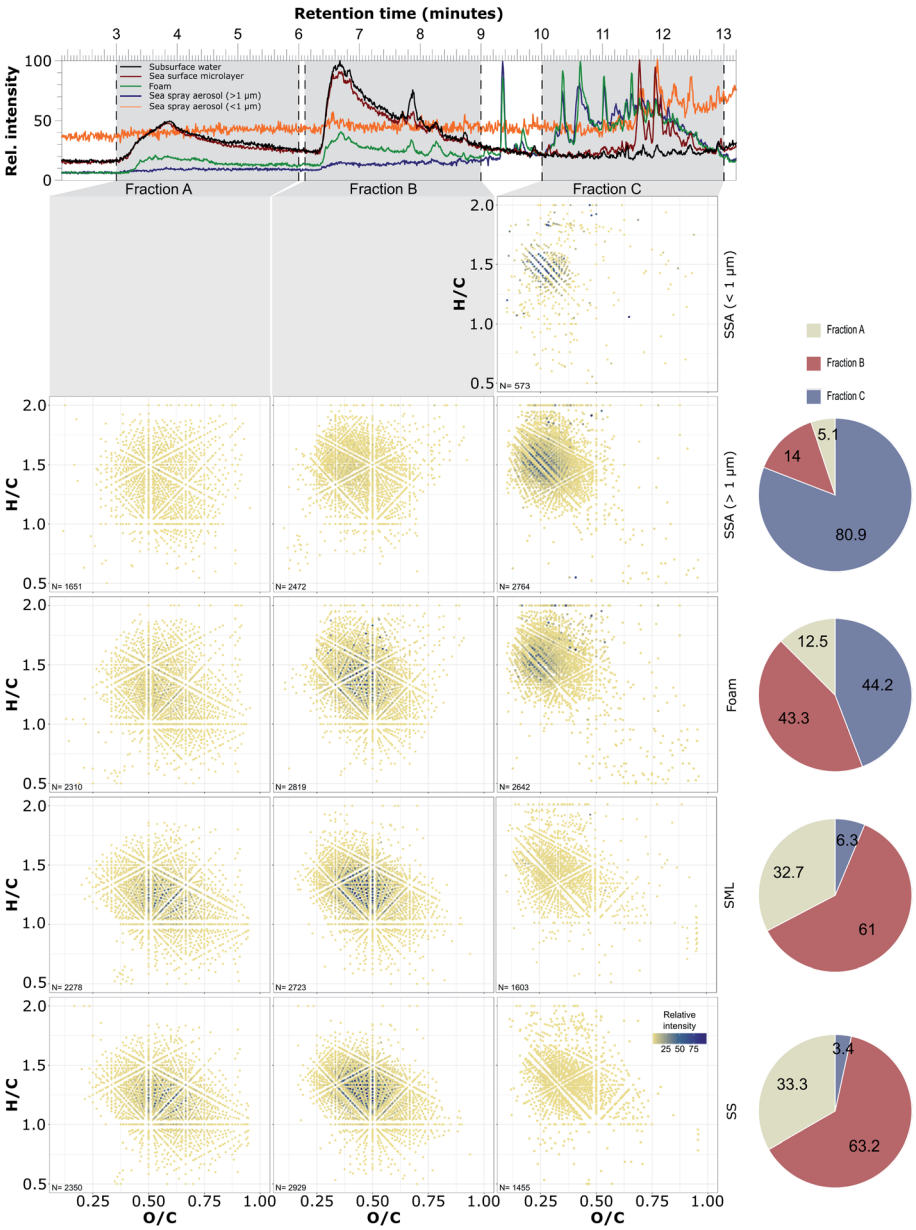

Fig. 1 The top panel presents a comparison of example normalised total ion chromatograms by mass spectrometry for SS, SML, foam and the sub- and supermicron SSA samples obtained on June 21st with polarity fractions divided *in silico* as indicated by the shaded areas (fraction *A*, fraction *B* and fraction *C*). Assigned ions for each polarity fraction were plotted in van Krevelen diagrams using their H/C and O/C atomic ratios. The colour scale represents ion intensities that have been normalised to the sum of the assigned ions from all 3 polarity fractions. "*N*" represents total number of assigned ions plotted for each fraction. Pie charts represent percentages of sums of all assigned ions' intensities for 3 polarity fractions.

supermicron fraction. For the least polar fraction *C*, which was the most abundant of the three fractions for both the submicron and the supermicron SSA, only 349 formulas were assigned in 5 out of 6 submicron SSA samples, compared to 1677 formulas assigned in 5 out of 6 supermicron samples (Fig. S5†). The average sum of all assigned ions in fraction *C* was 89 times lower for the submicron fraction compared to the supermicron fraction. Due to the very low ion abundancies, formulas were not assigned for polar fraction *A* and *B* in submicron SSA. Notably, the supermicron and submicron SSA exhibited similar molecular composition, with 73% of the compounds found in the submicron fraction also present in the supermicron fraction. That the overall signal was much lower for the submicron fraction than the supermicron fraction is unsurprising given that supermicron particles dominate the mass size distribution of nascent SSA [see *e.g.* ref. 1]. However, it is interesting that the submicron and supermicron fractions appeared so similar in terms of their composition given that smaller SSA have previously been shown to contain more surface-active compounds compared to larger SSA [ref. 79, *e.g.*]. Most likely, splitting the

SSA into only two fractions averaged out compositional differences with particle size.

That the abundance of the different fractions varied so much across the different sample types highlights the importance of fractionating the DOM prior to MS detection. Given that behind every detected molecular formula of DOM there is a complex mixture of structural isomers,[50–52] fractionation allows the partial separation of these mixtures into polarity fractions, improving the characterisation of samples. Further, this fractionation likely improved the sensitivity for compounds with lower abundance through decreased ion suppression inside the electrospray ionisation source.[57,59]

Compounds containing carboxylic acid functional groups are known to be abundant in marine DOM[48,51,80] and their retention on the C18 column is controlled by the low pH of the mobile phase A (0.1% formic acid) which keeps carboxylic acids in unionised form. As such, the gradual elution of the compounds observed in Fig. 1 is a result of the different number of carboxyl groups present, which is indicated by the changes in the average O/C and H/C values for each fraction (Table S7†). The most polar fraction, *A*, exhibited the highest O/C (0.54–0.56) and lowest H/C (1.2–1.4) ratios and likely consisted of highly unsaturated, carboxyl rich compounds. In contrast, the least polar fraction *C* had the lowest O/C (0.3–0.35) and highest H/C (1.4–1.5) ratios and was likely rich in more saturated compounds with a lower number of carboxyl groups. Comparison of the H/C ratios of the different sample types shows clearly that the weighted averages were lowest in the SS samples, increasing in the SML and foam samples to a maximum in the SSA samples. In contrast, the weighted average O/C ratios were at their maximum in the SS samples, decreasing in the foam and SML samples to a minimum in the SSA samples (Table S7†).

The most abundant compounds found in the SS and SML samples were spread over the more polar fractions *A* and *B* and had H/C ratios between 1–1.5 and O/C ratios between 0.3–0.7, which is in agreement with previous studies of marine DOM.[47,81] The majority of the compounds present in both the submicron and supermicron SSA samples had higher H/C and lower O/C values. The weighted average H/C and O/C values for the submicron SSA samples were 0.311 ± 0.007 and 1.508 ± 0.008 (mean $\pm$ SD) which was within the range obtained for the *C* fraction of supermicron SSA samples (Table S7†).

Previous studies probing the composition of the organic matter present in SSA have observed that it has higher H/C and lower O/C values[61,63] compared to subsurface seawater and this is in line with the results presented here showing a high abundance of the least polar fraction *C* in the SSA samples. Although the average H/C and O/C values we present here (Table S7†) are not directly comparable with studies that do not fractionate prior to MS identification, the average H/C and O/C values we observe for fraction *C* correspond remarkably well with the values observed in ambient marine aerosol collected over the Atlantic Ocean.[63]

The differences between the relative abundances in the three polarity fractions as well as the differences in the average H/C and O/C values between the different sample types highlight that it is the number of carboxyl groups that is the most significant factor in controlling the partitioning of DOM between the different sample types. A high abundance of polarity fractions *A* and *B* in the water samples is caused by a higher number of carboxyl groups (lower H/C and higher O/C) which more likely results in overall hydrophilic structure, decreasing the likelihood of a given molecular formula becoming enriched in SSA particles. On the other hand, a high abundance of polarity fraction *C* in the foam and SSA samples is the consequence of having less oxygenated molecules with fewer carboxyl groups which can result in a more surfactant-like structure: a part of the molecule that contains a hydrophilic functional group(s) and the rest of the molecule that is hydrophobic. Fatty acids and lipid-like molecules that are characterised by low O/C and high H/C ratios would be a proxy for this type of structure.[82] In addition to this, we can be almost certain that a higher abundance of non-polar moieties in these molecules makes them elute later, in the least polar fraction *C*, which makes this fraction representative for foam and SSA samples. This can be related to the study by Cavalli *et al.*[45] where a decrease in the surface tension measured in water extracts of SSA was linked to the structural properties of the identified organic molecules. These authors concluded that the presence of polar carbonyl functional groups (keto and carboxyl) together with hydrophobic aliphatic moieties probably results in a structure with surface-active properties that allows these molecules to be abundant in SSA.

For all four types of samples (SS, SML, foam and supermicron SSA) a trend of increasing weighted-average molecular weight with increasing retention time is apparent (Table S7†), which indicates that the non-polar character of compounds that elute later and are preferably transferred to SSA (fraction *C*) are not only influenced by the lower number of carboxyl groups, but also due to increased molecular weight. This is supported by the observation that it is fraction *C* of the supermicron SSA samples which has the highest average molecular weight (around 500 Da) with a much higher abundance of ions above 600 Da compared to fraction *C* of the SS and SML samples. Considering that compounds in fraction *C* have fewer carboxyl groups, this effect may be explained by the increased size of the non-polar fraction of the molecule which enhances its surface-active properties. This effect has been shown previously for different classes of surfactants with one functional group *e.g.* perfluoroalkyl acids (PFAAs) where increasing the chain length increases enrichment in SSA [*e.g.* ref. 83 and 84]. However, somewhat surprisingly, this contradicts the work of Schmitt-Kopplin *et al.*[61] who observed that the range of molecular weights in nascent SSA was lower compared to the subsurface water the aerosols were generated from. While the range of molecular weights observed in supermicron SSA in our study where generally higher than the range of molecular weights in the subsurface water we observed the opposite for submicron SSA where the range of molecular weights were lower than in the supermicron SSA (Fig. S8†). However, given the low mass of submicron SSA sampled we cannot rule out that this was an artefact of the sampling and analysis. Interestingly the range of molecular weights in fraction *C* of the supermicron aerosol is most similar to the range of molecular weights in fraction *C* of

the foam sample which again implies that the foam is a transition between the SML and SSA (Fig. S8†).

The extreme complexity of DOM precludes the use of authentic analytical standards and obtaining quantitative information about specific analytes, which is the main limitation of non-target approaches in general. However, many strategies are available to estimate the ionisation efficiency of the different compounds assigned using non-target LC-MS from which it is possible to draw certain quantitative conclusions.[85] It has been shown that the increasing chain length of carboxylic acids[86] and the decreasing area in the carboxylic acid molecule that is accessible to the polar solvent[87] improves their response in ESI sources. This is explained by their increased affinity to the surface of the electrospray droplets where nonpolar sections of the charged ions are already desolvated in the air which enhances their transfer to the gas phase, compared to overall hydrophilic ions that have more affinity towards the interior of the electrospray droplets. Improved ESI response was also found for the compounds that elute later in reversed-phase liquid chromatography[88] and have a higher logarithm of partition and distribution coefficient between octanol and water ($\log P$ and $\log D$)[89,90] which all corresponds to the increased nonpolar character of charged ions. However, some studies have failed to find a correlation between $\log P$ and negative ESI response.[91,92] Based on studies that found a correlation between molecular properties and ESI response, we could assume that compounds in the least polar fraction *C*, that are characteristic of SSA, and for which we presume stronger surface-active properties, will exhibit higher ionisation efficiencies compared to compounds in fractions *A* and *B*. Given this, the low relative abundance of compounds in fraction *C* of the SS and SML samples could suggest that the actual concentration of these compounds in these samples were also low.

The instrumental response of the same compound in the different types of samples obtained in this study can also be impacted by compounds which co-elute, something often referred to as matrix effects. Typically internal standards are used to quantify the impact of matrix effects on ESI response. However, the use of internal standards in non-targeted analysis, such as that utilised in the current study, is extremely complicated since organic matter is comprised of thousands of different compounds which can elute across a wide range of polarity fractions. Surface-active compounds are expected to produce more significant matrix effects since they will likely suppress the signal of the analytes through competitive mechanisms on charged ESI droplets.[87] Based upon this it is logical to conclude that the fraction of samples most impacted by this effect in the current study would be fraction *C* of the SSA samples. However, fraction *C* of the SSA samples exhibited a much higher number of assigned peaks compared to fraction *C* of the SS and SML samples. This supports the conclusion that the differences observed between the sample types are due to actual differences in concentrations rather than matrix effects. Another approach used to minimise and evaluate the impact of matrix effects is dilution of samples or injection of smaller sample volumes since this should decrease the concentration of compounds which may interfere with the analysis.[93,94] In the current study, injection of different volumes of the SSA samples (5–20 μL) did not result in higher variability than replicate injection with the same injection volume (BCD = 3–5% *vs.* BCD = 1–5%). Further, the standard deviation of the weighted average H/C and O/C values for different injection volumes of the SSA samples was 15 and 50 times lower than the standard deviation between different SSA samples for the H/C and the O/C values, respectively.

Although PPL has proven to be the most efficient sorbent for marine DOM extraction,[53] retention on the sorbent is shown to be weak for very polar compounds such as sugars and biopolymers, while some very non-polar compounds potentially remain on the column.[95] In addition to this, ESI is less efficient for very polar compounds like sugars and proteins.[96] For these reasons these classes of compounds are most probably underestimated in our results. For the SS and SML samples (polarity fraction *A* and *B*) the fraction of the total ion intensity that was assigned with unique molecular formulas was on average 70%. This is in line with the analysis of different humic substances with Orbitrap instruments that have the same or similar resolving power as the instrument used in this study.[56] For supermicron SSA samples (polarity fraction *C*) the fraction of peaks that were assigned was lower, representing 58% of total ion intensity. A significant number of unassigned peaks in all fractions were present in the lower mass range (<250 Da) and had relatively higher Kendric mass defects. These ions are common background contaminant ions and they represented the majority of ions in the blank samples. However, a significant number of unassigned peaks in SSA supermicron samples (polarity fraction *C*) were not present in blank samples and were characteristic for a mass range between 750–1000 Da, with Kendric mass defect > 0.5. These peaks were not assigned potentially due to poorer resolution in this mass range or because they potentially represent organic compounds with a higher number of heteroatoms that were not included in the formula assignment procedure.

3.2 Temporal trends in organic matter composition during a phytoplankton bloom

During the period of measurements the seawater chlorophyll-a (chl-a) concentration increased three-fold from approximately 1 μg L^{-1} to approximately 3 μg L^{-1} indicating that a phytoplankton bloom was underway. In fact this was only the beginning of the spring bloom which peaked at approximately 7 μg L^{-1} on July 2nd. This bloom was dominated by diatoms and notably the species *Guignardia delicatula* which increased in abundance and dominance as the bloom progressed (see Christiansen *et al.*[64] for further details). This is consistent with previous studies focused on spring and summer phytoplankton blooms on the Faroes shelf where a dominance of diatom species, with a gradual shift from larger to smaller and non-siliceous diatom species is usually observed.[65,67] Interestingly the progression of the bloom exhibited little impact on the organic matter fraction of the nascent SSA which ranged between 0.08 and 0.22 and between 0.005 and 0.008 for the submicron and the supermicron SSA, respectively with no clear trend during the campaign (see Christiansen *et al.*[64]).

It is immediately evident that more saturated (higher H/C values) and less oxygenated compounds (lower O/C values) were positively correlated with chl-a levels and that these compounds became more abundant as a result of the bloom (Fig. 2). In contrast, compounds with lower H/C and higher O/C values did not (they were negatively correlated with chl-a). This trend was apparent in all three polarity fractions but the highest percentage of correlated compounds with chl-a (78–85%) was observed for the least polar fraction *C* of the SML and SSA (Table S6†). The majority of the sum-normalised intensities in the submicron SSA were positively correlated with chl-a along with the presence of ions with H/C < 1 and ions with O/C > 0.5 which were not present in the supermicron aerosol (Fig. S5†). By removing these ions from the data set and normalising the ion intensities using only those ions that were present in both the sub- and super-micron aerosol fractions, the correlation between the remaining ions and chl-a in the submicron fraction suggests a similar molecular fingerprint pattern to the super-micron fraction (Fig. S4†). Temporal changes in the weighted average H/C and O/C values for the submicron samples also suggest that the significant increase in H/C and decrease in the O/C values occurred after the chl-a levels increased over 1.5 μg L^{-1}. That the relative abundance of compounds with the highest H/C and lowest O/C values (*i.e.* the lowest number of

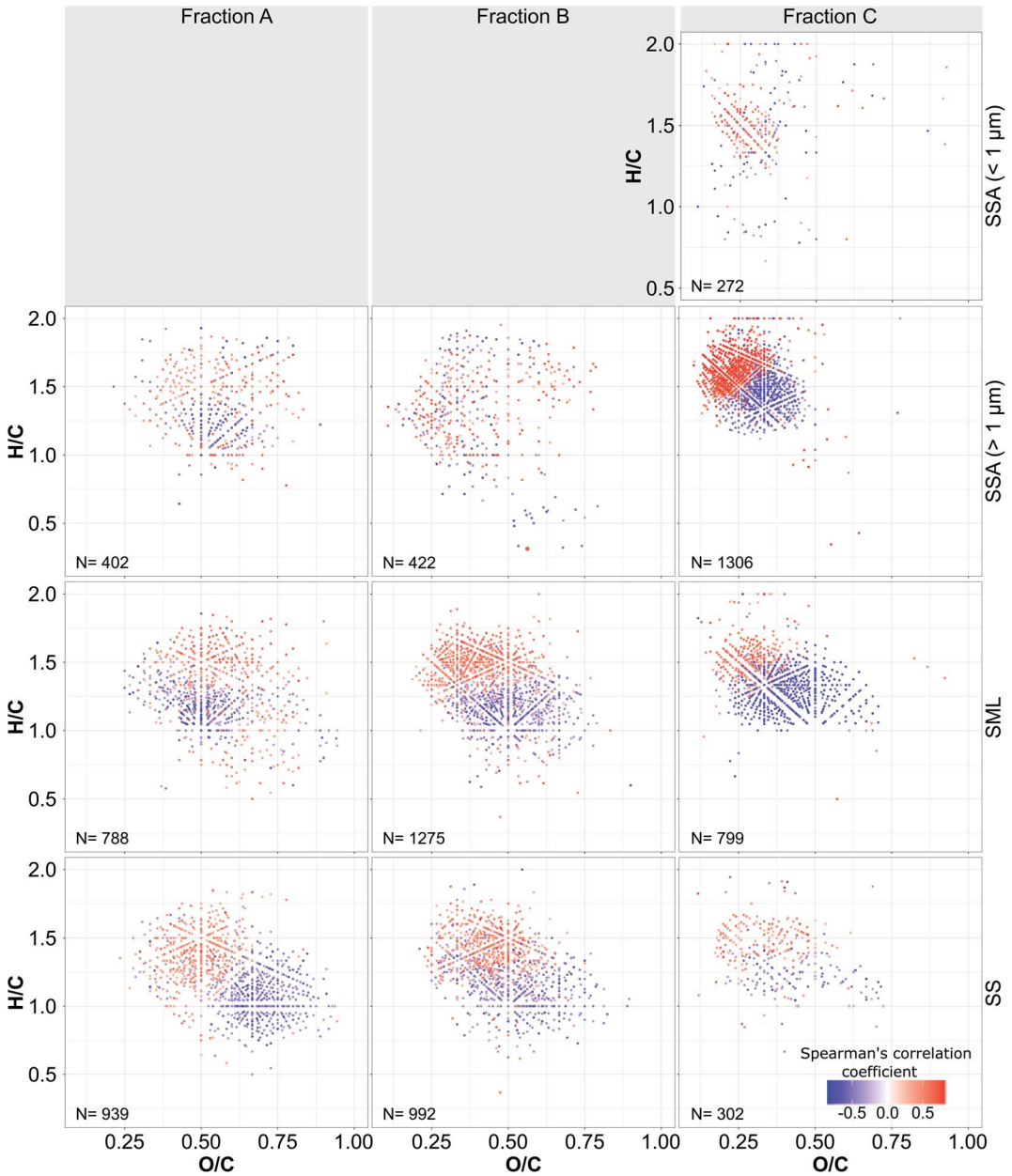

Fig. 2 Van Krevelen diagrams of molecular formulas plotted by their H/C and O/C atomic ratios, where the colour scale represents correlations (Spearman's coefficient) between their sum-normalised intensities and chl-a concentrations. Only compounds that show Spearman's coefficients >0.3 or ≤0.3 are plotted, "*N*" representing their total number.

carboxyl groups) increased during the bloom suggests that a significant amount of surface-active compounds were generated. This conclusion is further supported by the fact that the highest correlation between the weighted averaged H/C and O/C values and chl-a was found in the least polar fraction *C* of both the SML and SSA samples (Fig. S6 and S7†). Notably, although a high number of compounds that correlated with chl-a were also observed in the more polar fractions *A* and *B* in the SS and SML these changes were not reflected in the weighted average H/C and O/C values. This is most likely due to the fact that there was a high abundance of compounds in the more polar fractions of these samples that were unaffected by the bloom.

No molecular fingerprint pattern was observed for the compounds that are present in less than 10 of the SS and SML samples and less than 5 of the SSA samples. These compounds account for a very small percentage of total ion intensity (Table S6†) and are likely to be much more affected by instrumental noise. This is reflected in the lower repeatability of these compounds (Fig. S5†) and it probably resulted in higher uncertainty of the quantitative comparison for these compounds between different samples.

Since marine DOM is the product of various autochthonous and allochthonous sources it represents one of the most heterogeneous organic mixtures.[97] Although a large amount of fresh organic carbon is produced by photosynthesizing microorganisms most of this organic matter is rapidly consumed and modified so that DOM represents a mixture of different forms of labile and recalcitrant compounds.[98] By visualising the complex nature of DOM mass spectra using van Krevelen diagrams it is possible to assign certain regions of the diagram to a specific class of compounds.[82,99,100] The majority of the molecular formulas present in the most polar fraction *A* and a significant part of molecular formulas from polarity fraction *B* fall in the central part of the van Krevelen diagram that is attributed to carboxyl-rich alicyclic molecules (CRAM).[47,48] CRAM represents a significant portion of refractory organic matter and it is assumed that it contains microbially processed constituents of marine microbes' cell membranes.[47] Formulas with the highest H/C and lowest O/C values in the least polar fraction *C* are within the lipid-like region of the van Krevelen diagram, while the formulas with lower H/C and higher O/C ratios in polarity fraction *C* are spread over the protein-like and CRAM region.[47,48,54,82,100] For example, it has been shown that more labile, microbially derived compounds can be linked to lipid-, protein- and amino sugar-like regions of van Krevelen diagrams, with relatively high H/C (>1.5) and low O/C (<0.7) ratios.[99,101] In line with this previous work, our data show that it was the compounds with the highest H/C and lowest O/C values for each polar fraction which were positively correlated with biological activity. Most of these positively correlated compounds have H/C > 1.25, and O/C < 0.7.

3.3 Fragmentation and structural analysis of DOM compounds

In order to probe the composition of our samples more deeply we have conducted a series of fragmentation experiments. This analysis revealed an abundance of ions in the chosen mass range (*m*/*z* from 395 to 412.4) that exhibit neutral losses of 1–4CO_2 (decarboxylation) indicating the presence of significant amounts of carboxyl functional groups (Fig. 3). Following the neutral losses of CO_2, combined neutral losses of CO_2 with H_2O (Fig. S9†) and CH_3OH (Fig. S10†) are also identified. While the neutral loss of water is not specific and can originate from either alcohol or carboxylic functional group, loss of methanol most likely originates from the carboxylic ester functional group. Neutral losses of water and methanol could not be distinguished for some precursors given that the mass range of the precursors (17 Da) contained homologs (CH_2 mass difference) which correspond to the mass difference between the CH_3OH and H_2O neutral losses. Those fragments that could not be assigned to a unique precursor ion were removed from the data set.

That we observe an abundance of carboxyl groups and other neutral losses is in agreement with previous fragmentation studies of DOM compounds, including analysis of river fulvic acids, refractory deep ocean OM and microbially derived OM.[51,80,102] Indeed, a similar fragmentation pattern has been observed across studies of the DOM present in natural waters, despite diverse OM sources and the use of different precursor ions. This uniformity of DOM compounds is probably a consequence of the similar microbial and photochemical processes involved in the degradation of organic matter which results in a complex mixture containing compounds with very similar functionality albeit with different structural isomers.[51]

The fragmentation experiment showed that the maximum observed number of CO_2 neutral losses per one molecular formula ranges from 1–4 in all three polarity fractions across all sample matrices (*e.g.* SS, SML and supermicron SSA). Based on the proposed fragmentation mechanism of fulvic acid,[102] neutral loss of nCO_2 molecules would result in a fragment where negative charge is located on the remaining carboxyl or alcohol group, meaning that the number of carboxyl groups could be therefore n or $n + 1$. This would indicate that for the range of 1–4CO_2 neutral losses, the number of carboxyl functional groups per molecular formula would be between 1–5. As the polarity decreased, the composition of the acids identified in all three types of samples shifted towards compounds with fewer carboxyl groups which is indicated by a lower number of observed CO_2 losses. This shift reflects the changes in the O/C and H/C values for each polarity fraction (Table S7†). Overall, all three types of sample showed a very similar range of molecular formulas, with the same functional groups. This indicates the SS, SML and supermicron SSA contain a similar set of compounds albeit with very different relative abundances (*e.g.* Fig. 1).

Through comparison of the full scan analysis with the fragmentation experiment, it becomes clear that the fragmentation method achieved better sensitivity for compounds with higher O/C and lower H/C values, especially in fraction *C* of the SSA samples (*e.g.* Fig. 1 and 3). This was most likely because detection of these compounds is more difficult in full-scan mode due to their lower abundance. In addition, fewer molecular formulas with one or two CO_2 neutral losses were observed in the intermediate and high polarity fractions of the

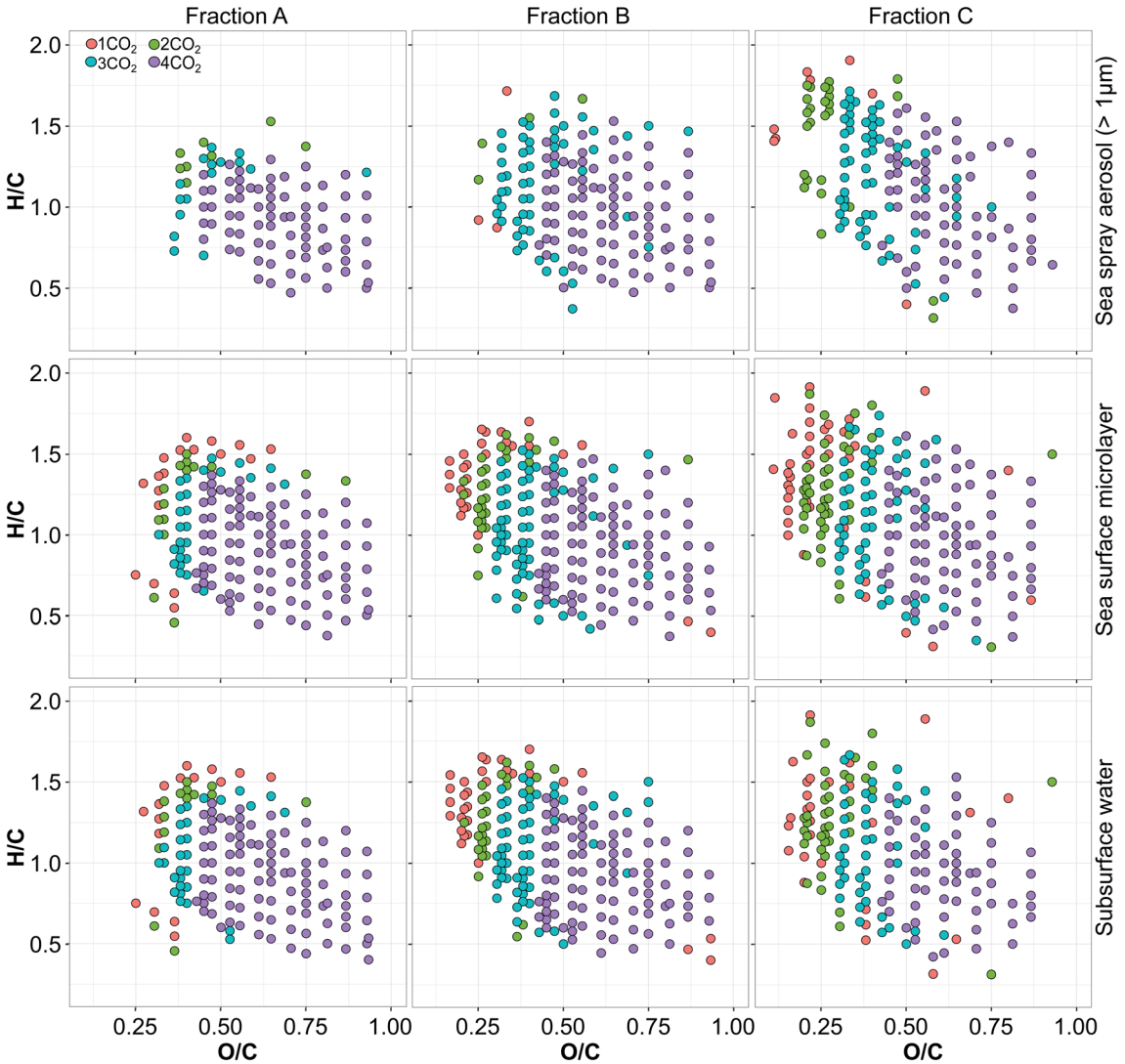

Fig. 3 Van Krevelen diagrams (H/C *vs.* O/C of identified molecular formulas) of DOM compounds assigned based on their detected fragment ions. The colours represent different types of neutral losses (from one to four CO_2 losses) that were observed for each molecular formula. When a molecular formula showed more than one type of neutral loss, data points were overlapped so that the colour shows the highest number of CO_2 losses observed. Results are based on the fragmentation of compounds in the mass range of *m*/*z* 395–412.

supermicron SSA samples. This was most likely due to the lower abundance of these fractions along with the improved sensitivity for compounds with more carboxyl groups.

The number of CO_2 losses we observed agreed well with the average O/C and H/C values (Fig. 3 and S9, S10†). Put simply, as the number of carboxyl groups increased, the molecule became more oxygen-rich (*i.e.* higher O/C) and the number of double bonds increased (*i.e.* lower H/C). This suggests that the assigned molecular formulas were a good predictor of the number of carboxyl groups for all three types of samples, which has been seen previously for deep-sea DOM compounds which represent the refractory fraction of DOM.[50]

3.4 The atmospheric relevance of our findings

Since the composition of the organic component of marine aerosol can influence aerosol direct and indirect effects on Earth's radiative budget characterising the composition of the organic matter present in nascent SSA is likely to be important for improved modeling of aerosol-climate effects in the marine environment. Although it is well established that biological activity in the ocean measurably impacts the organic composition of seawater[103,104] it remains unclear whether these changes are reflected in the composition of nascent SSA. Our findings suggest that the organic composition of nascent SSA does indeed reflect the organic composition of seawater as a result of changing biological activity in the water. Interestingly, while the composition of the organic fraction of the nascent SSA changed notably during the course of the measurements the enrichment of TOC in the aerosol was essentially unchanged during the bloom similar to previous studies [*e.g.* ref. 35 and 36].

The changes in the O/C and H/C ratios we observed during the bloom indicate a decrease in the abundance of carboxyl

groups. Although we have not measured the volatility, viscosity and light-absorbing properties of the aerosol, previous studies suggest that changes in the abundance of carboxyl groups can be linked to changes in these properties of aerosols.[105–107] Further, the increased abundance of oxygenated functional groups, detected as an increase of the O/C ratio or an increased abundance of COO fragments has previously been shown to increase the hygroscopicity of secondary aerosols particles.[108–110] As such, our observations of a decrease in the O/C ratio, or more specifically, an increase in the relative abundances of compounds with fewer carboxyl groups in nascent SSA during the phytoplankton bloom indicates the potential for the hygroscopicity of the aerosol to be reduced during phytoplankton blooms. However, it should be noted that previous laboratory studies suggest that the impact of biological activity on SSA hygroscopicity is relatively weak [*e.g.* ref. 111 and 112].

4 Conclusions

We have probed the composition of seawater and nascent SSA during the spring phytoplankton bloom in the North Atlantic using a novel liquid chromatography-mass spectrometry method. Our analysis revealed that the composition of DOM present in the seawater changed as the phytoplankton bloom progressed and that these changes were reflected in the composition of the organic matter present in the SSA. Further, the number and relative intensity of the compounds detected in the least polar fraction were both greater for SSA than in the seawater from which they were generated which highlights the selective nature of aerosolisation due to bubble-bursting.

The diatom bloom that occurred during our experiments resulted in the chl-a concentration increasing three-fold from approximately 1 $\mu g\ L^{-1}$ to approximately 3 $\mu g\ L^{-1}$. As this bloom progressed more saturated and less oxygenated compounds became significantly more abundant in the seawater. Although we observed this phenomena in all three of the polarity fractions we probed, this increase was clearly most abundant in the least polar fraction of the organic matter. This suggests that surface-active organic substances such as biogenic mono- and polycarboxylic acids and other biogenic organic substances were produced during the bloom. Importantly, the fact that these compositional changes were reflected in the nascent SSA we sampled provides strong evidence that the phytoplankton bloom which occurred had the potential to impact the composition of the SSA in the region with potential implications for its physicochemical properties and climate impact (*e.g.* cloud formation and cloud droplet stability). The agreement between the molecular O/C and H/C ratios with the identified number of carboxyl groups not only confirms their abundance in both seawater and aerosolised organic matter but also highlights their effect on the surface-active properties of the molecules, so that the compounds with fewer carboxyl groups (and other oxygen-containing functional groups) are selectively enriched in nascent SSA. The changes in the O/C and H/C ratios we observed during the bloom indicate a decrease in the abundance of carboxyl groups with potential impacts on the hygroscopicity, volatility, viscosity and light-absorbing properties of the aerosol.

Very few studies have used high-resolution mass spectrometry to investigate the composition of nascent SSA. As such, this study highlights the utility of this approach, both for characterising the composition of nascent SSA in general and for probing the impact of biogeochemical changes in seawater composition on SSA composition. Future work using this approach should aim at (i) increasing the size-resolution of the sampling such that the size-dependent composition of nascent SSA can be probed and (ii) probing the composition of ambient marine aerosol simultaneous to nascent SSA to determine whether changes in the biogeochemical state of the ocean are reflected in the ambient atmosphere and the extent to which nascent SSA may be driving these changes.

Author contributions

NR conducted the sample collection and extraction, mass spectrometry measurements and data analysis and led the writing of the manuscript. MS provided review of the results and their interpretation as well as manuscript editing. SC and MB planned and organised the overall field campaign. IC is the main supervisor of NR and obtained the funding for his PhD JJ, SC, JH, MB and IC all reviewed and provided editorial comments on the manuscript. All authors contributed to the article and approved the submitted version.

Conflicts of interest

There are no conflicts to declare.

Acknowledgements

We would like to thank Dr Ian Salter for proving the phytoplankton community composition data. MS and IC acknowledge funding from VR through projects 2016-05100 and 2016-04131. SC and MB acknowledges funding from the Faroese Research Council through project no. 0454. SC acknowledges the Carlsberg Foundation (CF20-0637). We also acknowledge Research Technician Erik Ejler Pedersen (Dept. of Chemistry, Aarhus University) for technical assistance during the campaign.

References

1 G. de Leeuw, E. L. Andreas, M. D. Anguelova, C. W. Fairall, E. R. Lewis, C. D. O'Dowd, M. Schulz and S. E. Schwartz, Production flux of sea spray aerosol, *Rev. Geophys.*, 2011, **49**, DOI: **10.1029/2010RG000349**.

2 D. M. Murphy, J. R. Anderson, P. K. Quinn, L. M. McInnes, F. J. Brechtel, S. M. Kreidenweis, A. M. Middlebrook, M. Pósfai, D. S. Thomson and P. R. Buseck, Influence of sea-salt on aerosol radiative properties in the southern ocean marine boundary layer, *Nature*, 1998, **392**(6671), 62–65.

3 A.-I. Partanen, E. M. Dunne, T. Bergman, A. Laakso, H. Kokkola, J. Ovadnevaite, L. Sogacheva, D. Baisnée, J. Sciare, A. Manders, *et al.*, Global modelling of direct

and indirect effects of sea spray aerosol using a source function encapsulating wave state, *Atmos. Chem. Phys. Discuss.*, 2014, **14**(4), DOI: 10.5194/acpd-14-4537-2014.

4 B. J. Finlayson-Pitts, The tropospheric chemistry of sea salt: A molecular-level view of the chemistry of nacl and nabr, *Chem. Rev.*, 2003, **103**(12), 4801–4822. ISSN 00092665.

5 A. H. Woodcock, Salt nuclei in marine air as a function of altitude and wind force, *J. Meteorol.*, 1953, **10**, 362–371.

6 F. Knelman, N. Dombrowski and D. M. Newitt, Mechanism of the bursting of bubbles, *Nature*, 1954, **173**, 261.

7 D. C. Blanchard, The electrification of the atmosphere by particles from bubbles in the sea, *Prog. Oceanogr.*, 1963, **1**, 73–112, DOI: 10.1016/0079-6611(63)90004-1.

8 D. E. Spiel, On the births of film drops from bubbles bursting on seawater surfaces, *J. Geophys. Res.*, 1998, **103**, 24907–24918, DOI: 10.1029/98JC02233.

9 J. C. Bird, R. De Ruiter, L. Courbin and H. A. Stone, Daughter bubble cascades produced by folding of ruptured thin films, *Nature*, 2010, **465**(7299), 759–762.

10 X. Jiang, L. Rotily, E. Villermaux and X. Wang, Submicron drops from flapping bursting bubbles, *Proc. Natl. Acad. Sci. U. S. A.*, 2022, **119**(1), e2112924119, DOI: 10.1073/pnas.2112924119. ISSN 0027-8424.

11 S. M. Burrows, O. Ogunro, A. A. Frossard, L. M. Russell, P. J. Rasch and S. M. Elliott, A physically based framework for modeling the organic fractionation of sea spray aerosol from bubble film langmuir equilibria, *Atmos. Chem. Phys.*, 2014, **14**(24), 13601–13629.

12 F. Macintyre, Geochemical fractionation during mass transfer from sea to air by breaking bubbles, *Tellus*, 1970, **22**(4), 451–462.

13 D. C. Blanchard, The ejection of drops from the sea and their enrichment with bacteria and other materials: A review, *Estuaries*, 1989, **12**, 127–137, DOI: 10.2307/1351816.

14 J. S. Lee, B. M. Weon, S. J. Park, J. H. Je, K. Fezzaa and W.-K. Lee, Size limits the formation of liquid jets during bubble bursting, *Nat. Commun.*, 2011, **2**(1), 367, DOI: 10.1038/ncomms1369. ISSN 2041-1723.

15 L. Duchemin, S. Popinet, C. Josserand and S. Zaleski, Jet formation in bubbles bursting at a free surface, *Phys. Fluids*, 2002, **14**(9), 3000–3008, DOI: 10.1063/1.1494072.

16 D. E. Spiel, The sizes of the jet drops produced by air bubbles bursting on sea- and fresh-water surfaces, *Tellus B*, 1994, **46**(4), 325–338, DOI: 10.3402/tellusb.v46i4.15808.

17 X. Wang, G. B. Deane, K. A. Moore, O. S. Ryder, M. Dale Stokes, C. M. Beall, D. B. Collins, M. V. Santander, S. M. Burrows, C. M. Sultana, *et al.*, The role of jet and film drops in controlling the mixing state of submicron sea spray aerosol particles, *Proc. Natl. Acad. Sci. U. S. A.*, 2017, **114**(27), 6978–6983.

18 D. V. Spracklen, S. R. Arnold, J. Sciare, K. S. Carslaw and C. Pio, Globally significant oceanic source of organic carbon aerosol, *Geophys. Res. Lett.*, 2008, **35**, DOI: 10.1029/2008GL033359.

19 E. Vignati, M. C. Facchini, M. Rinaldi, C. Scannell, D. Ceburnis, J. Sciare, M. Kanakidou, S. Myriokefalitakis, F. Dentener and C. D. O'Dowd, Global scale emission and distribution of sea-spray aerosol: Sea-salt and organic enrichment, *Atmos. Environ.*, 2010, **44**(5), 670–677.

20 K. Tsigaridis, N. Daskalakis, M. Kanakidou, P. J. Adams, P. Artaxo, R. Bahadur, Y. Balkanski, S. E. Bauer, N. Bellouin, A. Benedetti, T. Bergman, T. K. Berntsen, J. P. Beukes, H. Bian, K. S. Carslaw, M. Chin, G. Curci, T. Diehl, R. C. Easter, S. J. Ghan, S. L. Gong, A. Hodzic, C. R. Hoyle, T. Iversen, S. Jathar, J. L. Jimenez, J. W. Kaiser, A. Kirkevåg, D. Koch, H. Kokkola, Y. H. Lee, G. Lin, X. Liu, G. Luo, X. Ma, G. W. Mann, N. Mihalopoulos, J.-J. Morcrette, J.-F. Müller, G. Myhre, S. Myriokefalitakis, N. L. Ng, D. O'Donnell, J. E. Penner, L. Pozzoli, K. J. Pringle, L. M. Russell, M. Schulz, J. Sciare, Ø. Seland, D. T. Shindell, S. Sillman, R. B. Skeie, D. Spracklen, T. Stavrakou, S. D. Steenrod, T. Takemura, P. Tiitta, S. Tilmes, H. Tost, T. van Noije, P. G. van Zyl, K. von Salzen, F. Yu, Z. Wang, Z. Wang, R. A. Zaveri, H. Zhang, K. Zhang, Q. Zhang and X. Zhang, The aerocom evaluation and intercomparison of organic aerosol in global models, *Atmos. Chem. Phys.*, 2014, **14**(19), 10845–10895, DOI: 10.5194/acp-14-10845-2014. https://acp.copernicus.org/articles/14/10845/2014/.

21 D. R. Barker and H. Zeitlin, Metal-ion concentrations in sea-surface microlayer and size-separated atmospheric aerosol samples in Hawaii, *J. Geophys. Res.*, 1972, **77**, 5076–5086.

22 G. L. Hoffman and R. A. Duce, Alkali and alkaline earth metal chemistry of marine aerosols generated in the laboratory with natural seawaters, *Atmos. Environ.*, 1977, **11**, 367–372, DOI: 10.1016/0004-6981(77)90166-4.

23 C. Oppo, S. Bellandi, N. Degli Innocenti, A. M. Stortini, G. Loglio, E. Schiavuta and R. Cini, Surfactant components of marine organic matter as agents for biogeochemical fractionation and pollutant transport via marine aerosols, *Mar. Chem.*, 1999, **63**, 235–253, DOI: 10.1016/S0304-4203(98)00065-6. ISSN 0304-4203.

24 C. D. O'Dowd, M. C. Facchini, F. Cavalli, D. Ceburnis, M. Mircea, S. Decesari, S. Fuzzi, Y. J. Yoon and J. P. Putaud, Biogenically driven organic contribution to marine aerosol, *Nature*, 2004, **431**, 676–680, DOI: 10.1038/nature02959.

25 E. J. Hoffman and R. A. Duce, Organic carbon in marine atmospheric particulate matter: Concentration and particle size distribution, *Geophys. Res. Lett.*, 1977, **4**(10), 449–452.

26 A. Vaishya, J. Ovadnevaite, J. Bialek, S. Gerard Jennings, D. Ceburnis and C. D. O'Dowd, Bistable effect of organic enrichment on sea spray radiative properties, *Geophys. Res. Lett.*, 2013, **40**(24), 6395–6398.

27 Q. T. Nguyen, K. H. Kjær, K. I. Kling, T. Boesen and M. Bilde, Impact of fatty acid coating on the ccn activity of sea salt particles, *Tellus B*, 2017, **69**(1), 1304064.

28 D. T. McCoy, S. M. Burrows, R. Wood, D. P. Grosvenor, S. M. Elliott, P.-L. Ma, P. J. Rasch and D. L. Hartmann, Natural aerosols explain seasonal and spatial patterns of southern ocean cloud albedo, *Sci. Adv.*, 2015, **1**(6), e1500157.

29 P. J. DeMott, T. C. J. Hill, C. S. McCluskey, K. A. Prather, D. B. Collins, R. C. Sullivan, M. J. Ruppel, R. H. Mason, V. E. Irish, T. Lee, *et al.*, Sea spray aerosol as a unique source of ice nucleating particles, *Proc. Natl. Acad. Sci. U. S. A.*, 2016, **113**(21), 5797–5803.

30 E. J. Hoffman and R. A. Duce, Factors influencing the organic carbon content of marine aerosols: A laboratory study, *J. Geophys. Res.*, 1976, **81**(21), 3667–3670.

31 T. H. Bertram, R. E. Cochran, V. H. Grassian and E. A. Stone, Sea spray aerosol chemical composition: elemental and molecular mimics for laboratory studies of heterogeneous and multiphase reactions, *Chem. Soc. Rev.*, 2018, **47**(7), 2374–2400.

32 M. C. Facchini, M. Rinaldi, S. Decesari, C. Carbone, E. Finessi, M. Mircea, S. Fuzzi, D. Ceburnis, R. Flanagan, E. D. Nilsson, G. de Leeuw, M. Martino, J. Woeltjen and C. D. O'Dowd, Primary submicron marine aerosol dominated by insoluble organic colloids and aggregates, *Geophys. Res. Lett.*, 2008, **35**, DOI: **10.1029/2008GL034210**.

33 C. O'Dowd, D. Ceburnis, J. Ovadnevaite, J. Bialek, D. B. Stengel, M. Zacharias, U. Nitschke, S. Connan, M. Rinaldi, S. Fuzzi, *et al.*, Connecting marine productivity to sea-spray via nanoscale biological processes: Phytoplankton dance or death disco?, *Sci. Rep.*, 2015, **5**(1), 1–11.

34 M. Van Pinxteren, S. Barthel, K. W. Fomba, K. Müller, W. Von Tümpling, H. Herrmann and L. Thomsen, The influence of environmental drivers on the enrichment of organic carbon in the sea surface microlayer and in submicron aerosol particles–measurements from the atlantic ocean, *Elementa: Science of the Anthropocene*, 2017, **5**.

35 L. M. Russell, L. N. Hawkins, A. A. Frossard, P. K. Quinn and T. S. Bates, Carbohydrate-like composition of submicron atmospheric particles and their production from ocean bubble bursting, *Proc. Natl. Acad. Sci. U. S. A.*, 2010, **107**, 6652–6657, DOI: **10.1073/pnas.0908905107**.

36 P. K. Quinn, T. S. Bates, K. S. Schulz, D. J. Coffman, A. A. Frossard, L. M. Russell, W. C. Keene and D. J. Kieber, Contribution of sea surface carbon pool to organic matter enrichment in sea spray aerosol, *Nat. Geosci.*, 2014, **7**, 228–232, DOI: **10.1038/NGEO2092**.

37 T. Jayarathne, C. M. Sultana, C. Lee, F. Malfatti, J. L. Cox, M. A. Pendergraft, K. A. Moore, F. Azam, A. V. Tivanski, C. D. Cappa, *et al.*, Enrichment of saccharides and divalent cations in sea spray aerosol during two phytoplankton blooms, *Environ. Sci. Technol.*, 2016, **50**(21), 11511–11520.

38 V. Gerard, B. Noziere, C. Baduel, L. Fine, A. A. Frossard and R. C. Cohen, Anionic, cationic, and nonionic surfactants in atmospheric aerosols from the baltic coast at asko, sweden: Implications for cloud droplet activation, *Environ. Sci. Technol.*, 2016, **50**(6), 2974–2982.

39 A. A. Frossard, V. Gérard, P. Duplessis, J. D. Kinsey, X. Lu, Y. Zhu, J. Bisgrove, J. R. Maben, M. S. Long, R. Y.-W. Chang, S. R. Beaupré, D. J. Kieber, W. C. Keene, B. Nozière and R. C. Cohen, Properties of seawater surfactants associated with primary marine aerosol particles produced by bursting bubbles at a model air–sea interface, *Environ. Sci. Technol.*, 2019, **53**(16), 9407–9417, DOI: **10.1021/acs.est.9b02637**. PMID: 31329419.

40 M. V. Santander, J. M. Schiffer, C. Lee, J. L. Axson, M. J. Tauber and K. A. Prather, Factors controlling the transfer of biogenic organic species from seawater to sea spray aerosol, *Sci. Rep.*, 2022, **12**(1), 1–11.

41 D. Ceburnis, A. Masalaite, J. Ovadnevaite, A. Garbaras, V. Remeikis, W. Maenhaut, M. Claeys, J. Sciare, D. Baisnée and C. D. O'Dowd, Stable isotopes measurements reveal dual carbon pools contributing to organic matter enrichment in marine aerosol, *Sci. Rep.*, 2016, **6**(1), 1–6.

42 D. R. Crocker, R. E. Hernandez, H. D. Huang, M. A. Pendergraft, R. Cao, J. Dai, C. K. Morris, G. B. Deane, K. A. Prather and M. H. Thiemens, Biological influence on δ13c and organic composition of nascent sea spray aerosol, *ACS Earth Space Chem.*, 2020, **4**(9), 1686–1699.

43 S. R. Beaupré, D. J. Kieber, W. C. Keene, M. S. Long, J. R. Maben, X. Lu, Y. Zhu, A. A. Frossard, J. D. Kinsey, P. Duplessis, *et al.*, Oceanic efflux of ancient marine dissolved organic carbon in primary marine aerosol, *Sci. Adv.*, 2019, **5**(10), eaax6535.

44 A. A. Frossard, L. M. Russell, S. M. Burrows, S. M. Elliott, T. S. Bates and P. K. Quinn, Sources and composition of submicron organic mass in marine aerosol particles, *J. Geophys. Res.: Atmos.*, 2014, **119**(22), 12–977.

45 M. C. Cavalli, F. Facchini, S. Decesari, M. Mircea, L. Emblico, S. Fuzzi, D. Ceburnis, Y. J. Yoon, C. D. O'Dowd, J. P. Putaud and A. Dell'Acqua, Advances in characterization of size-resolved organic matter in marine aerosol over the North Atlantic, *J. Geophys. Res.*, 2004, **109**, DOI: **10.1029/2004JD005137**.

46 C. Deng, S. D. Brooks, G. Vidaurre and D. C. O. Thornton, Using raman microspectroscopy to determine chemical composition and mixing state of airborne marine aerosols over the pacific ocean, *Aerosol Sci. Technol.*, 2014, **48**(2), 193–206, DOI: **10.1080/02786826.2013.867297**.

47 N. Hertkorn, R. Benner, M. Frommberger, P. Schmitt-Kopplin, M. Witt, K. Kaiser, A. Kettrup and J. I. Hedges, Characterization of a major refractory component of marine dissolved organic matter, *Geochim. Cosmochim. Acta*, 2006, **70**(12), 2990–3010.

48 N. Hertkorn, M. Harir, B. P. Koch, B. Michalke and P. Schmitt-Kopplin, High-field nmr spectroscopy and fticr mass spectrometry: powerful discovery tools for the molecular level characterization of marine dissolved organic matter, *Biogeosciences*, 2013, **10**(3), 1583–1624.

49 S. K. Schum, L. E. Brown and L. R. Mazzoleni, Mfassignr: Molecular formula assignment software for ultrahigh resolution mass spectrometry analysis of environmental complex mixtures, *Environ. Res.*, 2020, **191**, 110114.

50 M. Zark, J. Christoffers and T. Dittmar, Molecular properties of deep-sea dissolved organic matter are

predictable by the central limit theorem: evidence from tandem ft-icr-ms, *Mar. Chem.*, 2017, **191**, 9–15.
51 M. Zark and T. Dittmar, Universal molecular structures in natural dissolved organic matter, *Nat. Commun.*, 2018, **9**(1), 1–8.
52 J. A. Hawkes, C. Patriarca, P. J. R. Sjöberg, L. J. Tranvik and J. Bergquist, Extreme isomeric complexity of dissolved organic matter found across aquatic environments, *Limnol. Oceanogr. Lett.*, 2018, **3**(2), 21–30.
53 T. Dittmar, B. Koch, N. Hertkorn and G. Kattner, A simple and efficient method for the solid-phase extraction of dissolved organic matter (spe-dom) from seawater, *Limnol. Oceanogr.: Methods*, 2008, **6**(6), 230–235.
54 J. D'Andrilli, T. Dittmar, B. P. Koch, J. M. Purcell, A. G. Marshall and W. T. Cooper, Comprehensive characterization of marine dissolved organic matter by fourier transform ion cyclotron resonance mass spectrometry with electrospray and atmospheric pressure photoionization, *Rapid Commun. Mass Spectrom.*, 2010, **24**(5), 643–650.
55 J. A. Hawkes, T. Dittmar, C. Patriarca, L. Tranvik and J. Bergquist, Evaluation of the orbitrap mass spectrometer for the molecular fingerprinting analysis of natural dissolved organic matter, *Anal. Chem.*, 2016, **88**(15), 7698–7704.
56 J. A. Hawkes, J. D'Andrilli, J. N. Agar, M. P. Barrow, S. M. Berg, N. Catalán, H. Chen, R. K. Chu, R. B. Cole, T. Dittmar, *et al.*, An international laboratory comparison of dissolved organic matter composition by high resolution mass spectrometry: Are we getting the same answer?, *Limnol. Oceanogr.: Methods*, 2020, **18**(6), 235–258.
57 C. Patriarca, J. Bergquist, P. J. R. Sjöberg, L. Tranvik and J. A. Hawkes, Online hplc-esi-hrms method for the analysis and comparison of different dissolved organic matter samples, *Environ. Sci. Technol.*, 2018, **52**(4), 2091–2099.
58 J. A. Hawkes, N. Radoman, J. Bergquist, M. B. Wallin, L. J. Tranvik and S. Löfgren, Regional diversity of complex dissolved organic matter across forested hemiboreal headwater streams, *Sci. Rep.*, 2018, **8**(1), 1–11.
59 L. Han, J. Kaesler, C. Peng, T. Reemtsma and O. J. Lechtenfeld, Online counter gradient lc-ft-icr-ms enables detection of highly polar natural organic matter fractions, *Anal. Chem.*, 2021, **93**(3), 1740–1748, DOI: 10.1021/acs.analchem.0c04426. PMID: 33370097.
60 Y. Qi, C. Ma, S. Chen, J. Ge, Q. Hu, S.-L. Li, D. A. Volmer and P. Fu, Online liquid chromatography and ft-icr ms enable advanced separation and profiling of organosulfates in dissolved organic matter, *ACS ES&T Water*, 2021, **1**(8), 1975–1982, DOI: 10.1021/acsestwater.1c00162.
61 P. Schmitt-Kopplin, G. Liger-Belair, B. P. Koch, R. Flerus, G. Kattner, M. Harir, B. Kanawati, M. Lucio, D. Tziotis, N. Hertkorn and I. Gebefügi, Dissolved organic matter in sea spray: a transfer study from marine surface water to aerosols, *Biogeosciences*, 2012, **9**(4), 1571–1582.
62 R. E. Cochran, O. Laskina, T. Jayarathne, A. Laskin, J. Laskin, P. Lin, C. Sultana, C. Lee, K. A. Moore, C. D. Cappa, *et al.*, Analysis of organic anionic surfactants in fine and coarse fractions of freshly emitted sea spray aerosol, *Environ. Sci. Technol.*, 2016, **50**(5), 2477–2486.
63 A. S. Willoughby, A. S. Wozniak and P. G. Hatcher, Detailed source-specific molecular composition of ambient aerosol organic matter using ultrahigh resolution mass spectrometry and 1h nmr, *Atmosphere*, 2016, **7**(6), 79.
64 S. Christiansen, N. Radoman, J. Johanson, I. Salter, S. Jacobson, H. B. Pedersen, T. Šantl Temkiv, I. Cousins, M. E. Salter and M. Bilde, Properties of sea spray aerosols during a spring phytoplankton bloom on the faroe shelf in the north atlantic, *Environ. Sci.: Atmos.*, in prep.
65 E. Gaard, B. Hansen and S. P. Heinesen, Phytoplankton variability on the Faroe Shelf, *ICES J. Mar. Sci.*, 8 1998, **55**(4), 688–696, DOI: 10.1006/jmsc.1998.0373. ISSN 10543139.
66 H. H. Debes and K. Eliasen, Seasonal abundance, reproduction and development of four key copepod species on the faroe shelf, *Mar. Biol. Res.*, 2006, **2**(4), 249–259, DOI: 10.1080/17451000600798787.
67 H. Debes, E. Gaard and B. Hansen, Primary production on the Faroe shelf: Temporal variability and environmental influences, *J. Mar. Syst.*, 2008, **74**(1–2), 686–697, DOI: 10.1016/j.jmarsys.2008.07.004.
68 B. Hansen, S. K. Eliasen, E. Gaard and K. M. H. Larsen, Climatic effects on plankton and productivity on the Faroe Shelf, *ICES J. Mar. Sci.*, 2005, **62**(7), 1224–1232, DOI: 10.1016/j.icesjms.2005.04.014.
69 E. Gaard and B. Hansen, Variations in the advection of Calanus finmarchicus onto the Faroe Shelf, *ICES J. Mar. Sci.*, 2000, **57**(6), 1612–1618, DOI: 10.1006/jmsc.2000.0962.
70 S. Christiansen, M. E. Salter, E. Gorokhova, Q. T. Nguyen and M. Bilde, Sea spray aerosol formation: Laboratory results on the role of air entrainment, water temperature, and phytoplankton biomass, *Environ. Sci. Technol.*, 2019, **53**(22), 13107–13116.
71 A. Järvinen, M. Aitomaa, A. Rostedt, J. Keskinen and J. Yli-Ojanperä, Calibration of the new electrical low pressure impactor (elpi+), *J. Aerosol Sci.*, 2014, **69**, 150–159.
72 G. W. Harvey, Microlayer collection from the sea surface: a new method and initial results, *Limnol. Oceanogr.*, 1966, **11**, 608–614.
73 T. Riedel and T. Dittmar, A method detection limit for the analysis of natural organic matter via fourier transform ion cyclotron resonance mass spectrometry, *Anal. Chem.*, 2014, **86**(16), 8376–8382.
74 J. J. Savory, N. K. Kaiser, A. M. McKenna, F. Xian, G. T. Blakney, R. P. Rodgers, C. L. Hendrickson and A. G. Marshall, Parts-per-billion fourier transform ion cyclotron resonance mass measurement accuracy with a "walking" calibration equation, *Anal. Chem.*, 2011, **83**(5), 1732–1736.
75 A. N. Kozhinov, K. O. Zhurov and Y. O. Tsybin, Iterative method for mass spectra recalibration via empirical estimation of the mass calibration function for fourier transform mass spectrometry-based petroleomics, *Anal. Chem.*, 2013, **85**(13), 6437–6445.

76 J. Rahlff, C. Stolle, H.-A. Giebel, N. I. H. Mustaffa, O. Wurl and D. P. R. Herlemann, Sea foams are ephemeral hotspots for distinctive bacterial communities contrasting sea-surface microlayer and underlying surface water, *FEMS Microbiol. Ecol.*, 2021, **97**(4), fiab035.

77 B. Velimirov, Sugar and lipid components in sea foam near kelp beds, *Mar. Ecol.*, 1982, **3**(2), 97–107.

78 S. K. Satpute, I. M. Banat, P. K. Dhakephalkar, A. G. Banpurkar and B. A. Chopade, Biosurfactants, bioemulsifiers and exopolysaccharides from marine microorganisms, *Biotechnol. Adv.*, 2010, **28**(4), 436–450.

79 D. K. Woolf, P. A. Bowyer and E. C. Monahan, Discriminating between the film drops and jet drops produced by a simulated whitecap, *J. Geophys. Res.: Oceans*, 1987, **92**(C5), 5142–5150, DOI: **10.1029/JC092iC05p05142**.

80 H. Osterholz, J. Niggemann, H.-A. Giebel, M. Simon and T. Dittmar, Inefficient microbial production of refractory dissolved organic matter in the ocean, *Nat. Commun.*, 2015, **6**(1), 1–8.

81 R. Flerus, O. Lechtenfeld, B. Koch, S. Mccallister, P. Schmitt-Kopplin, R. Benner, K. Kaiser and G. Kattner, A molecular perspective on the ageing of marine dissolved organic matter, *Biogeosciences*, 2012, **9**, 6, DOI: **10.5194/bg-9-1935-2012**.

82 S. Kim, R. W. Kramer and P. G. Hatcher, Graphical method for analysis of ultrahigh-resolution broadband mass spectra of natural organic matter, the van krevelen diagram, *Anal. Chem.*, 2003, **75**(20), 5336–5344.

83 J. H. Johansson, M. E. Salter, J. C. A. Navarro, C. Leck, E. D. Nilsson and I. T. Cousins, Global transport of perfluoroalkyl acids via sea spray aerosol, *Environ. Sci.: Processes Impacts*, 2019, **21**(4), 635–649.

84 B. Sha, J. H. Johansson, J. P. Benskin, I. T. Cousins and M. E. Salter, Influence of water concentrations of perfluoroalkyl acids (pfaas) on their size-resolved enrichment in nascent sea spray aerosols, *Environ. Sci. Technol.*, 2020.

85 A. Kruve, Strategies for drawing quantitative conclusions from nontargeted liquid chromatography–high-resolution mass spectrometry analysis, *Anal. Chem.*, 2020, **92**(7), 4691–4699, DOI: **10.1021/acs.analchem.9b03481**. PMID: 32134258.

86 B. A. Huffman, M. L. Poltash and C. A. Hughey, Effect of polar protic and polar aprotic solvents on negative-ion electrospray ionization and chromatographic separation of small acidic molecules, *Anal. Chem.*, 2012, **84**(22), 9942–9950, DOI: **10.1021/ac302397b**. PMID: 23066894.

87 L. Wu, Y. Wu, H. Shen, P. Gong, L. Cao, G. Wang and H. Hao, Quantitative structure–ion intensity relationship strategy to the prediction of absolute levels without authentic standards, *Anal. Chim. Acta*, 2013, **794**, 67–75.

88 N. B. Cech, J. R. Krone and C. G. Enke, Predicting electrospray response from chromatographic retention time, *Anal. Chem.*, 2001, **73**(2), 208–213, DOI: **10.1021/ac0006019**. PMID: 11199967.

89 T. Henriksen, R. K. Juhler, B. Svensmark and N. B. Cech, The relative influences of acidity and polarity on responsiveness of small organic molecules to analysis with negative ion electrospray ionization mass spectrometry (esi-ms), *J. Am. Soc. Mass Spectrom.*, 2005, **16**(4), 446–455, DOI: **10.1016/j.jasms.2004.11.021**.

90 K. R. Chalcraft, R. Lee, C. Mills and P. Britz-McKibbin, Virtual quantification of metabolites by capillary electrophoresis-electrospray ionization-mass spectrometry: Predicting ionization efficiency without chemical standards, *Anal. Chem.*, 2009, **81**(7), 2506–2515, DOI: **10.1021/ac802272u**. PMID: 19275147.

91 A. Kruve, K. Kaupmees, J. Liigand and I. Leito, Negative electrospray ionization via deprotonation: Predicting the ionization efficiency, *Anal. Chem.*, 2014, **86**(10), 4822–4830, DOI: **10.1021/ac404066v**. PMID: 24731109.

92 M. Oss, A. Kruve, K. Herodes and I. Leito, Electrospray ionization efficiency scale of organic compounds, *Anal. Chem.*, 2010, **82**(7), 2865–2872.

93 A. Kruve, I. Leito and K. Herodes, Combating matrix effects in lc/esi/ms: The extrapolative dilution approach, *Anal. Chim. Acta*, 2009, **651**(1), 75–80, DOI: **10.1016/j.aca.2009.07.060**, **https://www.sciencedirect.com/science/article/pii/S0003267009010162**.

94 C. Ferrer, A. Lozano, A. Agüera, A. Jiménez Girón and A. R. Fernández-Alba, Overcoming matrix effects using the dilution approach in multiresidue methods for fruits and vegetables, *Journal of Chromatography A*, 2011, **1218**(42), 7634–7639, DOI: **10.1016/j.chroma.2011.07.033**, **https://www.sciencedirect.com/science/article/pii/S0021967311010235**.

95 J. Raeke, O. J. Lechtenfeld, M. Wagner, P. Herzsprung and T. Reemtsma, Selectivity of solid phase extraction of freshwater dissolved organic matter and its effect on ultrahigh resolution mass spectra, *Environ. Sci.: Processes Impacts*, 2016, **18**, 918–927, DOI: **10.1039/C6EM00200E**.

96 S. Gan, P. Guo, Y. Wu and Y. Zhao, A novel method for unraveling the black box of dissolved organic matter in soils by ft-icr-ms coupled with induction-based nanospray ionization, *Environ. Sci. Technol. Lett.*, 2021, **8**(4), 356–361, DOI: **10.1021/acs.estlett.1c00095**.

97 D. A. Hansell and C. A. Carlson, Marine dissolved organic matter and the carbon cycle, *Oceanography*, 2001, **14**(4), 41–49, DOI: **10.5670/oceanog.2001.05**.

98 D. A. Hansell, Recalcitrant dissolved organic carbon fractions, *Ann. Rev. Mar. Sci*, 2013, **5**, 421–445.

99 J. D'Andrilli, W. T. Cooper, C. M. Foreman and A. G. Marshall, An ultrahigh-resolution mass spectrometry index to estimate natural organic matter lability, *Rapid Commun. Mass Spectrom.*, 2015, **29**(24), 2385–2401.

100 J. R. Laszakovits and A. A. MacKay, Data-based chemical class regions for van krevelen diagrams, *J. Am. Soc. Mass Spectrom.*, 2022, **33**(1), 198–202, DOI: **10.1021/jasms.1c00230**. PMID: 34874727.

101 M. P. Bhatia, S. B. Das, K. Longnecker, M. A. Charette and E. B. Kujawinski, Molecular characterization of dissolved

organic matter associated with the greenland ice sheet, *Geochim. Cosmochim. Acta*, 2010, **74**(13), 3768–3784.

102 M. Witt, J. Fuchser and B. P. Koch, Fragmentation studies of fulvic acids using collision induced dissociation fourier transform ion cyclotron resonance mass spectrometry, *Anal. Chem.*, 2009, **81**(7), 2688–2694.

103 C. A. Carlson, H. W. Ducklow and A. F. Michaels, Annual flux of dissolved organic carbon from the euphotic zone in the northwestern sargasso sea, *Nature*, 1994, **371**(6496), 405–408.

104 K. A. Prather, T. H. Bertram, V. H. Grassian, G. B. Deane, M. D. Stokes, P. J. DeMott, L. I. Aluwihare, B. P. Palenik, F. Azam, J. H. Seinfeld, *et al.*, Bringing the ocean into the laboratory to probe the chemical complexity of sea spray aerosol, *Proc. Natl. Acad. Sci. U. S. A.*, 2013, **110**(19), 7550–7555.

105 N. E. Rothfuss and M. D. Petters, Influence of functional groups on the viscosity of organic aerosol, *Environ. Sci. Technol.*, 2017, **51**(1), 271–279, DOI: **10.1021/acs.est.6b04478**. PMID: 27990815.

106 Y. Li, U. Pöschl and M. Shiraiwa, Molecular corridors and parameterizations of volatility in the chemical evolution of organic aerosols, *Atmos. Chem. Phys.*, 2016, **16**(5), 3327–3344, DOI: **10.5194/acp-16-3327-2016**. **https://acp.copernicus.org/articles/16/3327/2016/**.

107 S. M. Phillips and G. D. Smith, Light absorption by charge transfer complexes in brown carbon aerosols, *Environ. Sci. Technol. Lett.*, 2014, **1**(10), 382–386, DOI: **10.1021/ez500263j**.

108 P. Massoli, A. T. Lambe, A. T. Ahern, L. R. Williams, M. Ehn, J. Mikkilä, M. R. Canagaratna, W. H. Brune, T. B. Onasch, J. T. Jayne, *et al.*, Relationship between aerosol oxidation level and hygroscopic properties of laboratory generated secondary organic aerosol (soa) particles, *Geophys. Res. Lett.*, 2010, **37**(24), DOI: **10.1029/2010GL045258**.

109 L. Poulain, Z. Wu, M. D. Petters, H. Wex, E. Hallbauer, B. Wehner, A. Massling, S. M. Kreidenweis and F. Stratmann, Towards closing the gap between hygroscopic growth and ccn activation for secondary organic aerosols–part 3: Influence of the chemical composition on the hygroscopic properties and volatile fractions of aerosols, *Atmos. Chem. Phys.*, 2010, **10**(8), 3775–3785.

110 J. Duplissy, P. F. DeCarlo, J. Dommen, M. Rami Alfarra, A. Metzger, I. Barmpadimos, A. S. H. Prevot, E. Weingartner, T. Tritscher, M. Gysel, *et al.*, Relating hygroscopicity and composition of organic aerosol particulate matter, *Atmos. Chem. Phys.*, 2011, **11**(3), 1155–1165.

111 D. B. Collins, D. F. Zhao, M. J. Ruppel, O. Laskina, J. R. Grandquist, R. L. Modini, M. D. Stokes, L. M. Russell, T. H. Bertram, V. H. Grassian, G. B. Deane and K. A. Prather, Direct aerosol chemical composition measurements to evaluate the physicochemical differences between controlled sea spray aerosol generation schemes, *Atmos. Meas. Tech.*, 2014, **7**, 3667–3683.

112 S. Christiansen, L. Ickes, I. Bulatovic, C. Leck, B. J. Murray, A. K. Bertram, R. Wagner, E. Gorokhova, M. E. Salter, A. M. L. Ekman and M. Bilde, Influence of arctic microlayers and algal cultures on sea spray hygroscopicity and the possible implications for mixed-phase clouds, *J. Geophys. Res.: Atmos.*, 2020, **125**(19), e2020JD032808, DOI: **10.1029/2020JD032808**.